frontiers | Frontiers in Environmental Science

ORIGINAL RESEARCH
published: 11 May 2022
doi: 10.3389/fenvs.2022.873257

Fe-Sensitized Zeolite Supported TiO_2 for the Degradation of Tetracycline Using Blue LED Irradiation

Ghadeer Jalloul[1], Assi Al-Mousawi[1], Farah Chocr[1], Alaa Merhi[2], Hussein Awala[2] and Cassia Boyadjian[1]**

[1]Baha and Walid Bassatne Department of Chemical Engineering and Advanced Energy, Maroun Semaan Faculty of Engineering and Architecture, American University of Beirut, Beirut, Lebanon, [2]Laboratory of Inorganic and Organometallic Coordination Chemistry (LCIO), Faculty of Science, Lebanese University, Hadath, Lebanon

In this study, we investigated the photocatalytic degradation as a potential treatment of tetracycline (TC) antibiotic contaminated water using TiO_2 semiconductor. To expand the activity of TiO_2 into the visible light region and to enhance its adsorption capacity for TC, we explored its modification *via* sensitization with Fe ions and *via* immobilization on beta (BEA) zeolite support. The nano-sized beta zeolite, synthesized using the seed-assisted procedure, was used to immobilize TiO_2 initially prepared by the sol-gel method. The immobilized TiO_2/BEA catalyst was further ion exchanged with Fe^{3+} ions using $FeCl_3$ precursor. Fe^{3+} modified TiO_2/BEA (Fe-TiO_2/BEA) catalyst was characterized using SEM, XRD, BET, UV-VIS DRS, and FTIR. After the immobilization of TiO_2 over BEA, the surface area of TiO_2 increased from 90 to 530 m^2/g and similarly its TC adsorption efficiency increased from 10% to 33%. The photocatalytic performance of the Fe-TiO_2/BEA was evaluated under blue LED light for TC degradation. Fe-TiO_2/BEA exhibited higher TC removal efficiency (100%) compared to TiO_2 (80%) after 90 min of irradiation using 50 W blue LED light for a 250 mg/L initial catalyst concentration and 20 mg/L TC concentration. The enhanced performance of the final catalyst was a result of the expanded surface area due to the immobilization of the TiO_2 on the BEA zeolite, which resulted in an improved TC adsorption. Moreover, the presence of Fe^{3+} ions reduced the band gap energy of the TiO_2, hence led to a red shift in its absorption spectrum to the visible light region and minimized the extent of the recombination of the charge carriers.

Keywords: tetracycline, photocatalytic degradation, beta zeolite, immobilized TiO_2, Fe-sensitized TiO_2, blue LED light

OPEN ACCESS

Edited by:
Hyunook Kim,
University of Seoul, South Korea

Reviewed by:
Vincenzo Vaiano,
University of Salerno, Italy
Diana Sannino,
University of Salerno, Italy

****Correspondence:***
Hussein Awala
Hussein.awala@ul.edu.lb
Cassia Boyadjian
cb30@aub.edu.lb

Specialty section:
This article was submitted to Toxicology, Pollution and the Environment, a section of the journal Frontiers in Environmental Science

Received: *10 February 2022*
Accepted: *24 March 2022*
Published: *11 May 2022*

Citation:
Jalloul G, Al-Mousawi A, Chocr F, Merhi A, Awala H and Boyadjian C (2022) Fe-Sensitized Zeolite Supported TiO_2 for the Degradation of Tetracycline Using Blue LED Irradiation. Front. Environ. Sci. 10:873257. doi: 10.3389/fenvs.2022.873257

1 INTRODUCTION

Antibiotics (ABs) are antibacterial compounds used to treat bacterial infections both in humans and animals (Torres-Palma et al., 2020). Tetracyclines (TCs) are one of the most prescribed families of ABs and are widely used in medical, agricultural, and poultry sectors. TCs are poorly absorbed by the body (20%–50%), hence they are excreted to the environment *via* urine and feces (Liao et al., 2021). TCs continuous presence in the environment, both in water sources through urine and in soil through animal manure, have created adverse effects on the aquatic and agriculture ecosystems and have led to the development of antibiotic resistant bacteria (ARB) (Chong et al., 2015).

Photocatalytic degradation is an advanced oxidation process (AOP) that uses light activated catalysts for the removal of persistent organic contaminants from water (Chong et al., 2015; Saqib et al., 2019). Titanium dioxide (TiO_2) semiconductor has been reported to efficiently degrade ABs due to its attractive properties such as: high thermal and chemical stability, commercial availability, low cost and toxicity, and high specific surface (Foura et al., 2017; Behravesh et al., 2020; Ebrahimi et al., 2020). Nevertheless, several challenges limit the large-scale application of TiO_2 in the photocatalytic degradation of ABs under visible light: 1) TiO_2 has a band gap energy of (3.2 eV) which limits its activation to mere UV light that accounts only for 3%–5% of the solar spectrum, 2) TiO_2 nanoparticles used in slurry reactors require expensive, energy consuming, and complicated recovery for further reutilization, 3) the finely dispersed TiO_2 particles suffer from aggregation which hinders its efficiency in slurry reactors (Chong et al., 2015; Foura et al., 2017; Saqib et al., 2019; Behravesh et al., 2020; Hu et al., 2021). In order to red-shift TiO_2 light absorption, researchers have investigated several methods to decrease its band gap energy or to introduce new intra-band gap energy states *via* doping with transition metals such as Cr, Fe, Co, Mo, Mn, and V, or their ions (Foura et al., 2017). In metal doped-TiO_2, upon visible light excitation the electrons in the metal dopant are excited and are transferred to the conduction band of TiO_2 leading to its activation (Zhang et al., 2019). Specifically, iron metal-ion doping of TiO_2 can minimize the back recombination of electrons (e^-) and holes (h^+) and therefore maintain a high stable degradation efficiency (Foura et al., 2017; Saqib et al., 2019). Many studies in literature have reported on the visible light sensitization of TiO_2 *via* Fe metal ion doping. For example, Tsiampalis et al. (2019) reported successful degradation of the sulfamethoxazole antibiotic using 0.04% Fe/TiO_2 under simulated solar radiation. Furthermore, the UV-VIS DRS results confirmed an enhanced visible light absorption of the doped TiO_2 and a decrease in its band gap energy from 3.2 eV to around 2 eV with an increase in the Fe content from 0.04% to 2%. The visible light photocatalytic degradation efficiency of the metal ion doped TiO_2 was 95% after 90 min compared to only 45% by the undoped TiO_2. Another study by Suwannaruang et al. (2020) reported visible light induced degradation of ciprofloxacin AB over Fe-N-TiO_2 mesoporous photocatalyst using visible light emitting diode (LED) as illumination source. With the increase in Fe content, the morphology of the doped catalyst was gradually converted from spindle to spherical shape. For the same nitrogen content (2.5%), increasing the Fe content from 0.5% to 1.5% decreased the band gap energy of TiO_2 from 2.9 eV to 2.7 eV. Nearly, 70% of the antibiotic was removed after 6 h radiation compared to only 17% using the undoped TiO_2 (Suwannaruang et al., 2020).

TABLE 1 | BET specific surface area and external surface area (m^2/g) and micro and meso pore volumes (cm^3/g) of BEA, TiO_2, and Fe-TiO_2/BEA.

Sample	S_{BET}	V_{micro}	S_{ext}	V_{meso}	V_{total}	d
BEA	620	0.26	120	0.44	0.70	25
Fe-TiO_2/BEA	530	0.22	170	0.40	0.62	22
TiO_2	90	0.04	190	0.08	0.12	49

S_{BET}, specific surface area (m^2/g), V_{micro}, micropore volume (cm^3/g); S_{ext}, external surface area (m^2/g), V_{meso}, mesopore volume (cm^3/g); d, crystallite size (nm).

In addition to metal ion doping of TiO_2 for enhanced photocatalytic activity, immobilization of TiO_2 particles on porous and inert supports has been widely investigated by researchers to control its morphology and improve adsorption capacity for the organic pollutant. TiO_2 immobilization further improves its stability, and ease of recovery specially when applied in large-scale slurry reactors. Several inorganic TiO_2 immobilizing substrates such as magnetite core, activated carbon, clays, ceramic, silicates, sands, glass, carbon nanotubes, polymers, and zeolites have been investigated (Lei et al., 2012; Mozia et al., 2012; Bel Hadjltaief et al., 2015; Chong et al., 2015; Cunff et al., 2015; Nawawi et al., 2016; Foura et al., 2017; Wang et al., 2017; Cunha et al., 2018; Mohd Adnan et al., 2018; Oblak et al., 2018; Radwan et al., 2018; Mahdavi et al., 2019; Saiful Amran et al., 2019; Scaria et al., 2020; Hu et al., 2021). Among the mentioned supports, zeolites have gained superior attention due to their desirable properties such as: high specific area and excellent adsorption ability for pollutants (surface area: 350–950 m^2/g and pore volumes >0.1 cm^3/g) (Yilmaz et al., 2013). Beta zeolite (BEA) is one type of zeolite with an interesting architecture of 3D open framework pore structure, high adsorption ability, shape/size selective properties, high hydrothermal stability, easily reachable large micro-pore volume, wide pore channel network, and strong acid sites (Taufiqurrahmi et al., 2011; Yilmaz et al., 2013). Researchers have reported many examples on TiO_2/zeolite systems of enhanced photocatalytic activities due to the enhanced and stable adsorption of pollutants on the catalyst over long reaction times. Titania/zeolite composites have been investigated for the removal of various pollutants in water, including dyes and pharmaceuticals (Al-Harbi et al., 2015; Saadati et al., 2016a; Foura et al., 2017; Liu et al., 2017; Maksod et al., 2017; Rahman et al., 2018; Sun et al., 2018; Aghajari et al., 2019; Liu et al., 2019; Saqib et al., 2019; Behravesh et al., 2020). For antibiotics removal, Behravesh et al. (2020) prepared zeolite-supported TiO_2 to degrade acetaminophen and codeine pharmaceuticals under sunlight irradiation. The FTIR characterization confirmed the absence of chemical bonds between the TiO_2 and the support, while the SEM-EDX analysis combined with XRD patterns showed that TiO_2 particles were mainly uniformly dispersed on the external surface of the zeolite and partially in its pores. Zeolite immobilization of TiO_2 increased the surface area of TiO_2 from 50 m^2/g to 98 m^2/g, and therefore the photocatalyst was able to degrade 39% of the initial concentration of these pharmaceuticals after 120 min. In addition, Saadati et al. (2016b) used TiO_2-P25/Semnan natural zeolite for tetracycline degradation under visible light irradiation. The immobilized TiO_2-P25 exhibited a specific area of 93 m^2/g, which was two times larger than that of TiO_2-P25. This catalyst was able to degrade 87% of the initial tetracycline concentration within 90 min of radiation as compared to only 10% degradation efficiency by the TiO_2-P25. In this study, TiO_2 particles were deposited on the external sites of the zeolite leading to an

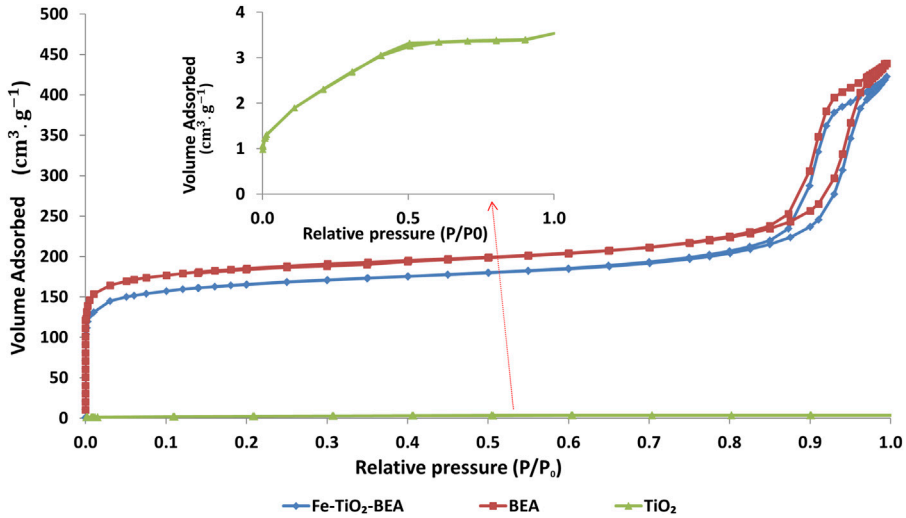

FIGURE 1 | N_2 adsorption-desorption isotherms at 77 K of BEA, TiO_2, and Fe-TiO_2/BEA. Inset: N_2 adsorption-desorption isotherms at 77 K of TiO_2.

improved adsorption of tetracycline. The XRD characterization of the final catalyst indicated that the structure of the zeolite was conserved and the crystallite size of TiO_2-P25 increased after the deposition of TiO_2 on zeolite, while the FTIR spectrum of the final catalyst exhibited a new absorption band proving the presence of a chemical bond between TiO_2 and the zeolite. The presence of such a chemical bond, however, was not always present in other reported TiO_2/zeolite systems (Foura et al., 2017; Maksod et al., 2017; Behravesh et al., 2020; López et al., 2021).

Additionally, both iron-modified and zeolite immobilized TiO_2 was used for the degradation of organic dyes under visible light. For example, Foura et al. (2017) used Fe-doped TiO_2 over HY zeolite for methylene blue degradation under visible light illumination and reported >98% removal efficiency after 60 min for the optimum 10 wt.% Fe-doped TiO_2/HY. In this particular work, FTIR characterization results indicated the absence of chemical interaction between the TiO_2 and the HY zeolite and BET analysis confirmed the deposition of TiO_2 in the pores of the zeolite. The UV-VIS DRS characterization proved that the addition of Fe into TiO_2/HY zeolite caused a red shift in its absorption spectrum towards the visible light region due a decrease in its band gap energy from 3.12 to 2.55 eV.

Recently, light-emitting diodes (LEDs) have gained interest in photocatalysis as efficient and economic light sources for the photocatalytic degradation of ABs and organic pollutants (Alpatova et al., 2015). The following characteristics of LEDs make them attractive for use: low power consumption, practical configuration, high energy efficiency, robustness, long life expectancy (50,000 h), flexibility of adjustment in various reactor designs (Casado et al., 2017; Liu et al., 2017). Many papers reported on the use of LEDs as efficient light sources for ABs removal in general (Malkhasian et al., 2014; Sarafraz et al.,

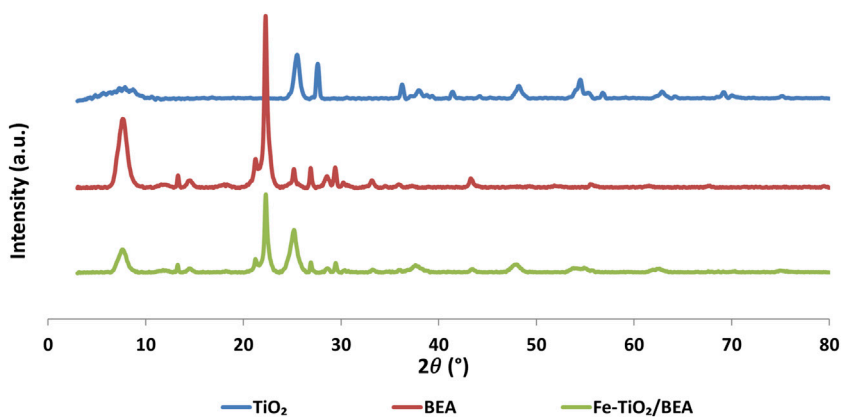

FIGURE 2 | XRD patterns of the prepared catalysts.

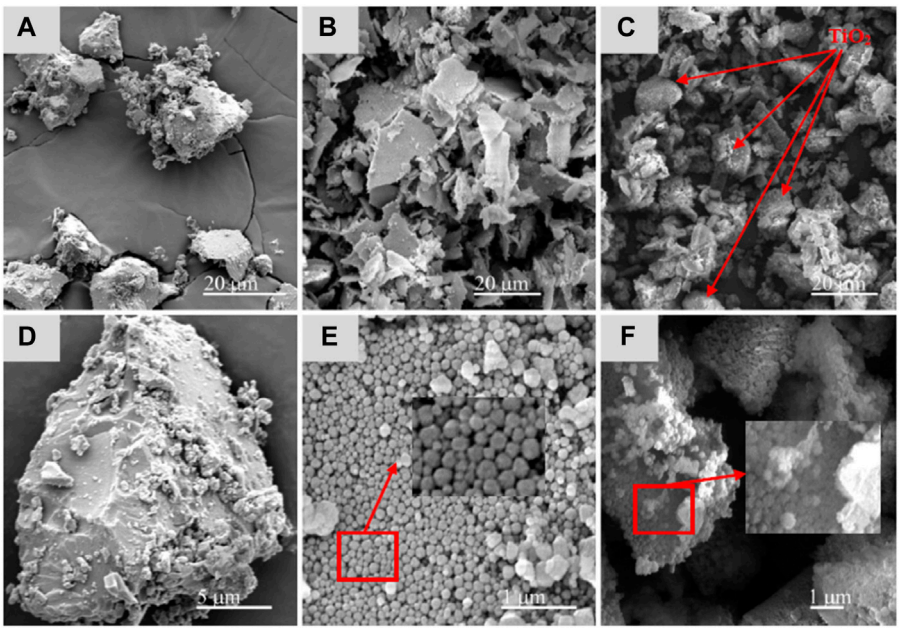

FIGURE 3 | SEM images at different magnification scales of TiO_2 **(A,D)**, BEA **(B,E)**, and Fe-TiO_2/BEA **(C,F)**.

2020; Zhong et al., 2020; AttariKhasraghi et al., 2021; Varma et al., 2021; Wang et al., 2021; Das and Ahn, 2022), and for tetracyclines removal in specific (Alpatova et al., 2015). For example Moshoeu et al. (2020), reported ~92% degradation efficiency of TC using TiO_2 nanofibers under LED strip with a wavelength ranging from UV to infrared region. Blue LED was also previously used to degrade TC using CdS semiconductor nanorods (Das and Ahn, 2022), where 92% efficiency was reported after 120 min for a 50 W lamp.

Particularly, the role of Fe ions has been investigated for the sensitization of TiO_2 under blue LED light ($420 < \lambda < 495$ nm). Impellizzeri et al. (2014) applied iron-modified TiO_2 in the form of Fe ion-implanted TiO_2 thin film for the photocatalytic degradation of methylene blue under blue LED light (420–470 nm). In this work, the introduced Fe ions lowered the band-gap energy of TiO_2 from 3.2 eV to 1.6–1.9 eV, resulting in an enhanced visible light absorption, hence in an improved photocatalytic efficiency. Similarly, both Tsiampalis et al. (2019) and Foura et al. (2017) modified titania *via* iron ion doping, and successfully expanded its activity to the visible light range between 420 and 490 nm.

In this work, we investigated both Fe^{3+} ion sensitization and zeolite immobilization routes to enhance the photocatalytic activity of TiO_2 for the degradation of tetracycline antibiotic under blue LED light. Sol-gel synthesized TiO_2 was immobilized on beta zeolite and further ion exchanged with iron. The structural, morphological and visible light properties of the prepared Fe-ion-exchanged BEA/TiO_2 (Fe-TiO_2/BEA) catalyst was studied in relation to the observed photocatalytic performance. Moreover, in order to achieve optimum degradation efficiency of the prepared catalyst for TC removal, the effect of various process conditions such as initial TC concentration, catalyst's concentration and light intensity were studied.

2 MATERIALS AND METHODS

2.1 Materials

LUDOX® SM colloidal silica 30 wt.% suspension SiO_2 in H_2O, (Sigma-Aldrich, 30%, particle size 3–4 nm), sodium hydroxide (Sigma-Aldrich), aluminium iso-butoxide (Sigma-Aldrich, 97%), tetraethylammonium hydroxide (Sigma-Aldrich, 35%), Titanium (IV) n-butoxide (Alfa Aesar), ethanol (Fisher Chemical, 99%), nitric acid (BDH Laboratory supplies, 69%), sodium hydroxide (Sigma-Aldrich), Tetracycline (Sigma-Aldrich), Iron (III) anhydrous chloride (BDH Laboratory supplies). All chemicals were used without further purification.

2.2 Preparation of the Catalysts

2.2.1 Preparation of TiO_2 Sol-Gel

TiO_2 was prepared using the sol-gel method as described previously (Bazargan et al., 2012). A mixture (A) of 4 ml of titanium (IV) butoxide and 2 ml of ethanol was stirred for 30 min. A second mixture (B) composed of 0.4 ml of nitric acid, 2 ml H_2O and 17 ml of ethanol was simultaneously prepared. Mixture (B) was gradually added into mixture (A) using a dropper (approximately 3 ml/min) under vigorous stirring for an hour during after which the clear solution turned into a gel. The obtained gel was then dried in an oven at 80°C for 3 h to remove traces of ethanol and H_2O. Then the dried sample was subjected to calcination in a muffle furnace for 4 h at 450°C to induce crystallization of TiO_2. The crystalline mass obtained after calcination was approximately 0.6 g.

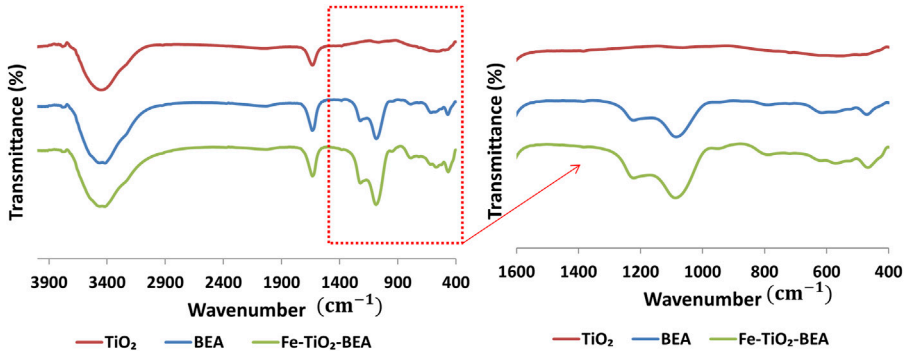

FIGURE 4 | FTIR of TiO_2, BEA, and Fe-TiO_2/BEA. Inset: Magnified FTIR of TiO_2, BEA, and Fe-TiO_2/BEA.

2.2.2 Preparation of BEA Zeolite

BEA zeolite was prepared *via* seed assisted approach. The BEA seeds were prepared from clear precursor suspensions with molar compositions: 9TEAOH: $0.5Al_2O_3$: $25SiO_2$: $295H_2O$, where TEAOH stands for tetraethylammonium hydroxide (Sigma-Aldrich, 35%). Initially, aluminium iso-butoxide (Sigma-Aldrich, 97%) was dissolved in a solution containing TEAOH and distilled water, and then the Silica source, colloidal Silica (LUDOX® SM 30 wt.%), was added into the mixture under stirring. After mixing the precursor suspensions for 60 min, a hydrothermal treatment was carried out at 100°C for 3 days. The obtained crystalline suspensions were purified by multistep high-speed centrifugation (20,000 rpm, 60 min); then the solid product was dried at 40°C and calcined at 550°C prior to being used as seeds.

The synthesis of BEA zeolite was carried out using the following suspension: $9.5Na_2O$:$0.25Al_2O_3$:$40SiO_2$:$570H_2O$ by dissolving LUDOX® SM colloidal silica (30 wt.% SiO_2, pH = 10, Aldrich) in a sodium hydroxide solution followed by heating at 100°C for 5–7 min in order to transform the turbid solution into clear water suspension. After cooling down to ambient temperature, BEA seeds (8 wt.%) were slowly added to the solution, and the mixture was homogenized by vigorous stirring for 30 min, followed by the addition of aluminum isopropoxide (Sigma-Aldrich, 98%). The obtained precursor suspension was further homogenized for 20 min before being transferred into a stainless-steel autoclave and subjected to the hydrothermal treatment at 100°C for 5 days under static condition. The resulting product was filtered, washed, and purified by double deionized water and then dried at 50°C. The yield of the sample was calculated with respect to the SiO_2, Al_2O_3, and the BEA seeds were included. A yield between 18 and 22% was obtained for BEA zeolites.

2.2.3 Modification of the TiO_2 Sol-Gel (Preparation of Fe-TiO_2/BEA Zeolite)

TiO_2/BEA Zeolite was prepared *in-situ* during the synthesis of the TiO_2 sol-gel, as previously reported (Sponza and Koyuncuoglu, 2019). After the preparation of TiO_2 sol-gel suspension, an appropriate amount of BEA zeolite nanoparticles was added into the transparent sol-gel to obtain 20% TiO_2/Zeolite composite. The obtained suspension was kept under stirring for 24 h. The final product was dried at 80°C for about 3 h followed by calcination at 450°C for 4 h. The as-synthesized zeolite supported TiO_2 (TiO_2/BEA) was then subjected to ion exchange treatment. Typically, 1.0 g of BEA/TiO_2 composite was stirred in 40 ml of 0.05 M iron chloride ($FeCl_3$) solution. The exchange process was repeated three times by separating supernatant from the mother liquid, re-dispersing it in new solution and repeating the procedure with the aforementioned ion exchange process to ensure that the highest possible exchange was achieved. The obtained sample after ion-exchange was washed thoroughly with double deionized water then dried in an oven at 80°C for 4 h followed by calcination in a muffle furnace at 450°C for 4 h. The final obtained sample was named Fe-TiO_2/BEA.

2.3 Characterization and Analysis Methods

Various analysis techniques were applied to characterize the surface morphology, structure and optical properties of each of the Fe-TiO_2/BEA, TiO_2, and BEA. Fourier transform infrared (FTIR) spectra in the range of 400–4,000 cm^{-1} were obtained using JASCO FTIR 6300 spectrometer using DTGS detector (resolution 4, 128 scans; KBr: sample = 99:1 mg) to study the structure of the prepared catalysts. X-ray powder diffraction (XRD) (BRUKER, D8) was used for the identification of crystalline phases. Fe-TiO_2/BEA, TiO_2, and BEA were analyzed in the range of $5^\circ < 2\theta < 80^\circ$ with a step size of 0.02°. The Scherrer Formula (**Eq. 1**) was used to calculate the average crystallite size of all samples;

$$d = \frac{0.89\lambda}{\beta cos\theta} \quad (1)$$

where d is the average crystallite size, λ is wavelength of the X-ray, 0.89 is the Scherrer's constant, β is the broadening at half the maximum intensity, and θ is the diffraction angle (Ali et al., 2017). **Table 1** presents results of these calculations**.** Scanning electron microscope (SEM) using MIRA3 LMU by TESCAN was used to investigate the morphology and structure of the three samples. Brunauer–Emmett–Teller (BET) coupled with

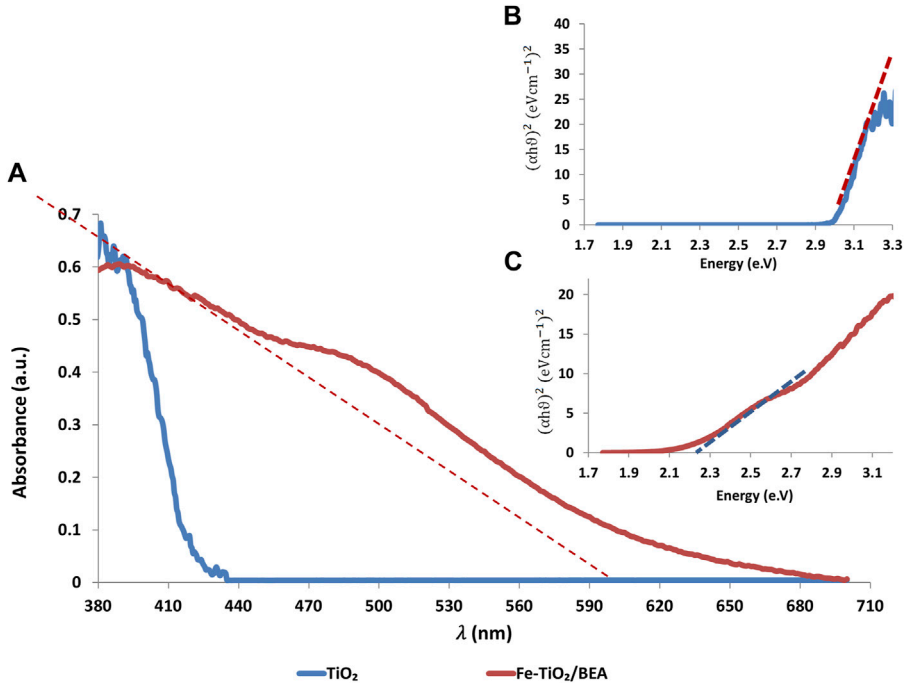

FIGURE 5 | (A): UV-VIS DRS of TiO_2 and Fe-TiO_2/BEA. Inset: Tauc's plots of **(B)**: TiO_2 and **(C)**: Fe-TiO_2/BEA.

Dubinin–Radushkevich method was used for the analysis and calculation of the surface area and pore volume of all samples. Nitrogen adsorption/desorption isotherms at 77 K (GEMINI VII 2390) in the relative pressure (P/P_0) range of 0.04–0.99 were applied. Diffuse reflectance spectroscopy (UV-VIS DRS) using (JASCO, V-570) in the range ($350 < \lambda < 700$ nm) was applied to study the optical properties of the prepared samples. To estimate the band gap energy of the samples, Tauc's formula (**Eq. 2**) was applied using the absorbance data of the UV-VIS DRS plot; where, α is the absorption coefficient, α_0 and h are constants, n is constant with a value of 0.5 or 2 for indirect and direct band gap semiconductors respectively, and (Eg) is the band gap energy of the sample. To find E_g, a linear plot of $(\alpha\ h\vartheta)^2$ vs. $h\vartheta$ is extrapolated ($n = 2$) and Eg estimated from the x-intercept (Khairy and Zakaria, 2014; Saadati et al., 2016b).

$$\alpha = \frac{\alpha_0\left(h\vartheta - E_g\right)^n}{h\vartheta} \tag{2}$$

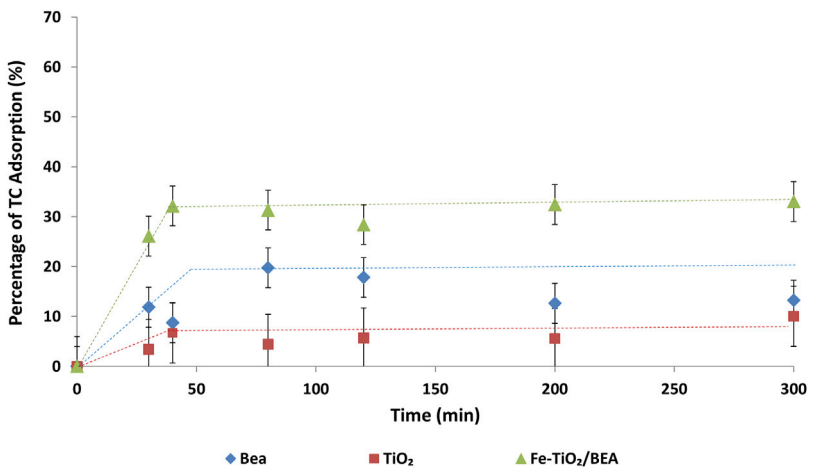

FIGURE 6 | Adsorption percentage of TC (20 mg/L) on BEA, TiO_2, and Fe-TiO_2/BEA (250 mg/L).

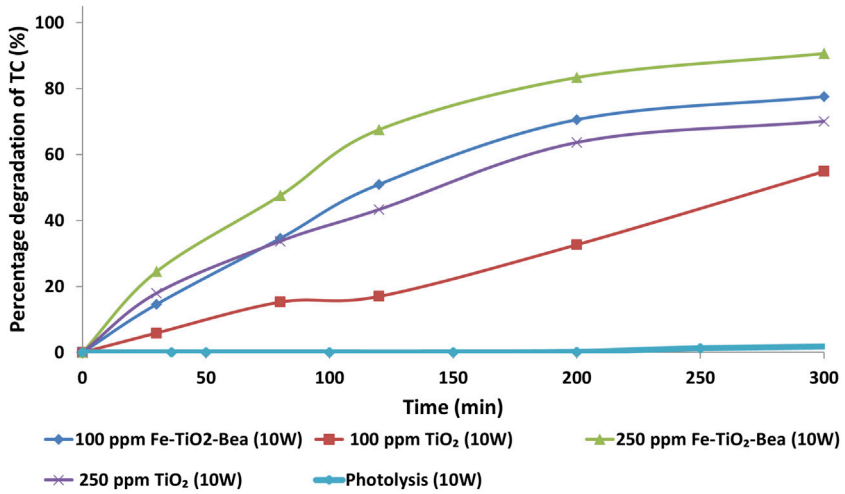

FIGURE 7 | The photolysis and photocatalytic degradation efficiencies of TC (20 mg/L) by TiO_2 and Fe-TiO_2/BEA catalysts at catalyst concentrations of 100 and 250 mg/L.

2.4 Photocatalytic Degradation Experiments

The photocatalytic degradation setup was composed of a 500 ml reactor beaker containing the TC solution and the photocatalyst. A blue LED light ($450 < \lambda < 495$ nm), used as the light source, was mounted at the top of the 500 ml beaker. The reactor was initially filled with 300 ml of TC solution with different weights of the photocatalysts; 30 mg or 75 mg of TiO_2 or Fe-TiO_2/BEA to obtain 100 mg/L and 250 mg/L initial concentration of the catalyst. The reaction mixture was kept at ambient conditions under stirring at 700 rpm. Prior to photocatalytic tests, the reactor was kept in the dark for 30 min to ensure adsorption/desorption equilibrium of TC on the catalyst's surface after which the light was turned on. A 2 ml sample was taken at pre-determined times (30, 40, 80, 120, 200, and 300 min), transferred into a Falcon tube and then centrifuged at 10,000 rpm for 15 min. High performance liquid chromatography (HPLC) (Agilent Technologies with ChemStation software), was used to analyze the concentration of the TC using a calibration curve previously prepared for TC. To calculate the degradation efficiency of each catalyst **Eq. 3** was applied, where C_0 and C_t are the initial and final concentration of TC at time t, respectively (Saadati et al., 2016a). Adsorption tests were performed using the same procedure as the photocatalytic degradation tests, but the reactor was kept in dark during the entire experiment without any use of light.

$$TC\ degradation\ \% = \frac{C_0 - C_t}{C_0} \times 100 \tag{3}$$

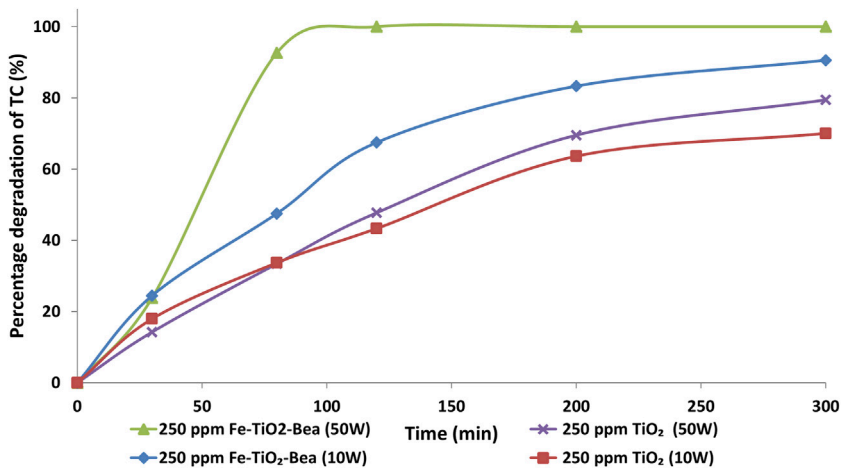

FIGURE 8 | The photocatalytic degradation efficiencies of TC (20 mg/L) by TiO_2 and Fe-TiO_2/BEA under 10 and 50 W light power.

TABLE 2 | Previous photocatalytic degradation work using zeolite immobilized titania.

Catalyst	Pollutant	Source of light	Efficiency	References and year
Zeolite immobilized TiO_2	Methylene blue dye	compact fluorescent light (36 W 400 < λ <750 nm)	92% after 180 min	Saqib et al. (2019) 2019
Fe-doped TiO_2 over HY zeolite	Methylene blue dye	Visible light	>98% 60 min	Foura et al. (2017) 2017
Au- modified TiO_2-BEA	Malachite green dye	Visible light	92% after 60	Maksod et al. (2017) 2017
TiO_2-Fe_2O_3/Fe-doped zeolite X	Oxytetracycline antibiotic	200 W 455 nm LED	98% after 60 min	Liu et al. (2019) 2019
TiO_2-Fe_2O_3/zeolite with persulfate	Ciprofloxacin antibiotic	50 W 455 nm LED	100% after 3.5 h	Liu et al. (2017) 2017
TiO_2-P25/Semnan natural zeolite	Tetracycline antibiotic	Visible irradiation	87% in 90 min	Saadati et al. (2016b) 2016
Ag-TiO_2 supported by artificial zeolite	Methylene blue dye	500 W high-pressure xenon light cut-off wavelength of 420 nm	93% within 90 min	Sun et al. (2018) 2018
Fe-TiO_2/BEA	Tetracycline	50 W Blue LED (450 < λ <495 nm)	100% after 90 min	Our work

3. RESULTS AND DISCUSSION

3.1 Characterization of the Catalysts

3.1.1 Specific Surface Area

Figure 1 shows the N_2 adsorption-desorption isotherms at 77 K of each of the BEA, TiO_2, and Fe-BEA/TiO_2 sample. The adsorption-desorption isotherm of the BEA nanocrystals showed a combination between Type I and Type IV isotherms. The isotherm was demonstrated by a steep uptake of N_2 gas at the low partial pressure due to the presence of micropores, followed by a plateau and a slight inclination with the increase in the partial pressure and was terminated with a large hysteresis loop at the relatively high partial pressure. Such a feature was associated with textural pores formed by the close packing of mono dispersed and well-shaped nanosized crystallites, which gave rise to the characteristic mesoporous structure of the BEA. The N_2 adsorption-desorption isotherm of the Fe-BEA/TiO_2 showed a comparable result to that of the BEA zeolite, while TiO_2 did not show any microporous structure with a pore volume of only 0.08 cm^3/g. This was a clear evidence that, in the Fe-BEA/TiO_2, no additional micropores were added to the BEA zeolite nanoparticles and the mesoporous structure of the BEA was preserved without any changes in its morphology or intergrowth as a result of TiO_2 dispersion.

As shown in **Table 1**, the calculated Brunauer-Emmett-Teller (BET) surface area of BEA zeolite was 620 m^2/g while its total pore volume was 0.70 cm^3/g. The BET surface area and the total pore volume of the Fe-TiO_2/BEA were 530 m^2/g and 0.62 cm^3/g, respectively. The decrease in the BET surface area of the final catalyst is explained by TiO_2 dispersion in its micropores leading to a partial blockage of these pores. Our results were in accordance with literature studies (Liu et al., 2018; Shokrolahi et al., 2019); for example, Shokrolahi et al. (2019) and Liu et al. (2018) reported that TiO_2 deposition on the surface and in the pores of the zeolite reduced its surface area and pore volume. Similarly, Foura et al. (2017) concluded that the specific surface area of the zeolite support decreased linearly as the amount of immobilized TiO_2 increased. This happened due to partial clogging of the micro-pores of zeolite as TiO_2 could enter these pores. In contrast, as demonstrated in N_2 sorption, we observed a huge increase in the external surface area of the BEA from 120 to 170 m^2/g in the Fe-TiO_2/BEA catalyst. This was in agreement with previous work (Tayade et al., 2007; Sun et al., 2018; Liu et al., 2019; Behravesh et al., 2020) and confirmed that TiO_2 dispersion occurred mainly on the external surface of the zeolite and only partially in its pores. The external surface area of a zeolite/TiO_2 composite was previously reported to increase when TiO_2 particles were dispersed on the external surface of the zeolite and not in its internal pores (Saadati et al., 2016b). This happened when the pore diameter of the zeolite was too small for TiO_2 molecules to enter.

3.1.2 X-Ray Powder Diffraction

Figure 2 shows the XRD patterns of BEA zeolite, TiO_2, and Fe-TiO_2/BEA catalysts. The XRD pattern of the zeolite substrate exhibited two main diffraction peaks at $2\theta = 7.6^\circ$ (75%) and 22.4° (100%). These peaks were in agreement with those of BEA zeolite, according to JCPDS 48-0038 standard and confirmed that our prepared zeolite exhibited nanocrystallite size as reported by Maksod et al. (2017). The XRD patterns of TiO_2 showed diffraction peaks at $2\theta = 25^\circ$ (80%), 37.9°, 48.2°, 55° (44%), and 62.5°, corresponding to the (101), (200), (211), (004), and (204) crystallographic planes for anatase phase, and 27° (80%), 36°, and 41.0°, corresponding to (110), (101), and (111) crystallographic planes of rutile phase according to spectrum standards (JCPDS 21-1272) and (JCPDS 21-1276). These results showed that our sol-gel prepared TiO_2 was mainly present in anatase polymorph with small portion present in rutile polymorph (Ebrahimi et al., 2020; Rahman et al., 2018; Saadati et al., 2016b; López et al., 2021; Liu et al., 2018). According to Kanakaraju et al. (Kanakaraju et al.,

2014), a mixture of anatase and rutile phases was obtained when calcining at intermediate temperatures 200°C < T < 550°C. For the modified catalyst, Fe-TiO_2/BEA, the obtained X-ray diffraction patterns showed characteristic diffraction peaks of the BEA zeolite both at 2θ = 7.6° (31%) and 22.4° (100%) and that of TiO_2 at 2θ = 25° (54%). This confirmed that both TiO_2 and zeolite were well incorporated in the final catalyst, and that the framework structure of the zeolite remained unmodified after the deposition of TiO_2 and after the ion exchange with Fe^{3+} ions, which is in well agreement with previous studies on TiO_2/zeolites (Saqib et al., 2019; Foura et al., 2017; Maksod et al., 2017; Liu et al., 2019; Liu et al., 2017; Saadati et al., 2016a; López et al., 2021; Shokrolahi et al., 2019; Liu et al., 2018; Tayade et al., 2007). Also, as obvious from XRD, Fe-TiO_2/BEA catalyst exhibited peaks at lower intensities than those of the BEA zeolite. This was further confirmed from the calculations of the crystallite sizes. As shown in **Table 1**, the average crystallite size of the TiO_2 based on the Scherrer Equation was found to be 49 nm while the average crystallite size of BEA was 25 nm. After the immobilization of TiO_2 on zeolite, the average crystallite size of the final catalyst was 22 nm, which was lower than the values of both TiO_2 and BEA. Moreover, the differences in the XRD peak ratios of the unmodified and modified TiO_2, could be attributed to a decrease in the phase transition of the TiO_2 in the final catalyst, from the anatase to the rutile phase. The absence of peaks associated to the presence of any crystalline iron oxide phases in the XRD spectra, was due to the low iron content (less than 5 wt.%), hence to the small crystallite sizes of these iron phases, which stayed below the detection limit of XRD (Ali et al., 2017).

3.1.3 Scanning Electron Microscope (SEM)

Figure 3 shows the SEM images at different magnification scales of all the prepared samples. The SEM images of the BEA zeolite showed rough sphere-shaped surfaces contributing to its high surface area and making it an excellent adsorbent for many organic molecules (Liu et al., 2018; Liu et al., 2019). The SEM images of the Fe-BEA/TiO_2 catalyst confirmed the distribution of TiO_2 on the surface of the BEA zeolite as nanoparticles and clusters, in well agreement with previously reported studies on zeolite immobilized TiO_2 (Saadati et al., 2016b; Liu et al., 2019; López et al., 2021). Based on the shown SEM images, we may also confirm that TiO_2 immobilization was nearly uniform over the entire surface of the zeolite leaving no uncovered exposed sites. The SEM characterization also indicated that although the surface of the BEA zeolite exhibited higher roughness upon immobilization with TiO_2, its morphology and structure remained unchanged. The same observations were previously reported by Saadati et al. (2016b) and Aghajari et al. (2019).

3.1.4 FTIR Spectroscopy

In order to demonstrate the nature of the interaction of TiO_2 with the zeolite in the photocatalyst, samples were characterized by FTIR. **Figure 4** presents the FTIR spectra of the Fe-TiO_2/BEA in reference to both unmodified BEA and TiO_2 samples. The intense vibration obtained in the spectrum of the BEA zeolite at 3,730 cm^{-1} corresponds to the stretching and bending of OH present at the surface of the inorganic material (Foura et al., 2017; Liu et al., 2018), while peaks at the 1,634 cm^{-1} region are attributed to the bending vibration of H–O–H bonds of the adsorbed water molecules, as reported in various literature articles (Foura et al., 2017; Maksod et al., 2017; Liu et al., 2018; Rahman et al., 2018; Ebrahimi et al., 2020). The band at 950–1,250 cm^{-1} corresponds to the antisymmetric stretching vibration of the Si(Al)-O in the tetrahedral $Si(Al)O_4$ skeleton of the zeolite (Taufiqurrahmi et al., 2011; Saadati et al., 2016b; Foura et al., 2017; Liu et al., 2018; Behravesh et al., 2020). The observed band at the 520–570 cm^{-1} range corresponds to the T–O, T–O–T, and O–T–O (T: Si or Al atom) symmetric stretching vibrations and confirms the presence of ring-shaped tetrahedral SiO_4 and AlO_4 units (Taufiqurrahmi et al., 2011; El-Sherbiny et al., 2014; Foura et al., 2017; Maksod et al., 2017; Liu et al., 2018). In general, the observed vibration bands in the FTIR spectra of the BEA zeolite, corresponding to Si, Al, and O bonds, confirmed the successful synthesis of the BEA zeolite and illustrated the degree of crystallinity of the zeolite substrate along with the order of its structure (Maksod et al., 2017). The FTIR spectrum of the TiO_2, showed two clear peaks, a broad peak at 3,500 cm^{-1} corresponding to the symmetric and asymmetric stretching vibrations of the hydroxyl group (Ti–OH) of the TiO_2 particles and another at 1,634 cm^{-1} corresponding to the bending vibrations of adsorbed water molecules (Praveen et al., 2014; Maksod et al., 2017). The FTIR spectrum of the final catalyst Fe-TiO_2/BEA, showed new peaks at the 945 to 900 cm^{-1} range that might correspond to anti-symmetric stretching vibrations of Ti–O–Si and Ti-O-Al as similarly reported by Li et al. (2005). The conserved FTIR peaks of the zeolite BEA in the final catalyst indicated that the structure of the zeolite was stable and partially affected by the TiO_2 immobilization, which led to the formation of Ti-O-Si or Ti-O-Al, and this confirmed the incorporation of Ti in the zeolite structure in the final sample. The incorporation of Ti was due to the high calcination temperature, which caused the condensation of Si-OH or Al-OH bond with Ti-OH.

3.1.5 UV-VIS DRS Analysis

Figure 5 represents the UV-VIS diffuse reflectance spectra of Fe-TiO_2/BEA and TiO_2 applied to study the optical properties of the catalysts BEA, Fe, and TiO_2. The wavelength of the spectral onset increased from around 400 nm for TiO_2 to around 595 nm for the modified TiO_2 in a similar manner as reported previously for iron-modified TiO_2 (Foura et al., 2017; Tsiampalis et al., 2019; Ali et al., 2017). The light absorbance of the final Fe-TiO_2/BEA catalyst in the visible region of the light spectrum (400–575 nm) was higher than that of unmodified TiO_2. **Figure 5** presents the Tauc's plot of both the TiO_2 and the Fe-TiO_2/BEA photocatalysts. The band gap energy of TiO_2 was found to be 3.05 eV and was found to decrease to 2.23 eV after its immobilization on the BEA zeolite and applying the ion exchange process of the iron ions. We attribute this decrease in the band gap energy and eventually the increase in visible light absorption of the final catalyst, to the presence of the Fe^{3+} ions on the Fe-BEA/TiO_2 in a similar manner as reported in other studies (Impellizzeri et al., 2014; Foura et al., 2017). We propose that, during the ion exchange process of the BEA/TiO_2 with $FeCl_3$,

Fe^{3+} ions replaced the sodium compensating ions in the BEA zeolite, and since TiO_2 was dispersed on the zeolite (confirmed by SEM images), we propose that Fe^{3+} ions were also impregnated on the surface of TiO_2. Since XRD results confirmed the absence of any changes in the TiO_2 lattice parameters of the Fe-TiO_2/BEA catalyst, we confirm that the improved visible light absorption of the final catalyst was due to the role of the Fe^{3+} ions in reducing the band gap energy of the TiO_2 as confirmed by Tauc's plots and resulting in a red shift in its absorption spectrum to the visible light region (Ali et al., 2017; Maksod et al., 2017).

3.2 Experimental Results

3.2.1 Adsorption of Tetracycline

During photocatalytic degradation process, pollutants migrate into the surface of the catalyst and adsorb on it, then they are mineralized and eventually desorbed from the surface of the catalyst (Ibhadon and Fitzpatrick, 2013). In fact, poor adsorption of TC on the surface of the catalyst can limit the rate of the adsorption; hence eventually limit the rate of the degradation. **Figure 6** presents the adsorption of TC antibiotic on each of the BEA, TiO_2, and Fe-TiO_2/BEA under dark conditions, at room temperature with a catalyst dose of 250 mg/L. The obtained adsorption patterns by all samples followed the Langmuir adsorption isotherm, similar to what has been reported earlier by Liu et al. (2018). The Langmuir adsorption assumes a monolayer homogeneous adsorption that attains equilibrium saturation when a molecule occupies only a vacant adsorption site (Foo and Hameed, 2010), and the adsorption isotherm is characterized by an initial linear increase followed by a plateau reflecting the attained equilibrium saturation. After 300 min, the adsorption percentage of the tetracycline was the highest (33%) for the Fe-TiO_2/BEA. Our observations were in agreement with the work of Liu et al. (2018) who also reported enhanced overall adsorption percentages of sulfadiazine antibiotic onto TiO_2/zeolite compared to those of unmodified zeolite. In our work, the immobilization of TiO_2 over BEA zeolite enhanced its adsorption capacity for TC from 10% to 33%. This was mainly due to the higher specific surface area (530 m^2/g) of the Fe-TiO_2/BEA catalyst as compared to TiO_2 (90 m^2/g). Similar results were reported in previous studies (Saadati et al., 2016b; Saqib et al., 2019), where TC adsorption over TiO_2 was enhanced after the dispersion of TiO_2 photocatalyst over the zeolite support.

3.2.2 Photocatalytic Degradation of Tetracycline

3.2.2.1 Effect of the Initial Concentration of the Catalyst

Figure 7 shows the photolysis and photocatalytic degradation of tetracycline over TiO_2 and Fe-TiO_2/BEA under 10 W blue LED light at two different initial concentrations of the catalyst; 100 and 250 mg/L. The photolysis results indicated that nearly no TC was degraded in the absence of any catalyst under 10 W blue LED light. Almeida et al. (2022) reported no photodegradation of TC under visible light while Zarazua et al. (2017) reported very low degradation efficiency (~15%) of TC photolysis. As shown in **Figure 7**, at all catalyst concentrations, Fe-TiO_2/BEA resulted in higher degradation efficiency of the TC than the unmodified TiO_2 at both 100 mg/L (77% compared to 54%) and 250 mg/L (90% compared to 70%) initial catalyst loading. Based on our obtained results, we could deduce that both the Fe-metal ion insertion and the zeolite support immobilization enhanced the degradation activity of the TiO_2 under blue LED light. The simultaneous presence of Fe^{3+} ion exchanged zeolite of a large surface area synergistically enhanced the efficiency of the final catalyst by improving its TC adsorption and enhancing its visible light absorption (Foura et al., 2017). Previous studies (Ali et al., 2017; Foura et al., 2017) reported enhanced photocatalytic activity of the Fe-modified TiO_2 under visible light by the presence of the Fe^{3+} ions. For example, Foura et al. (2017) reported that Fe-modification of TiO_2/zeolite enhanced its photocatalytic degradation activity (98% after 60 min) for methylene blue dye under visible light as compared to TiO_2/zeolite (30% after 60 min). An optimum concentration of the Fe-dopant was reported to be crucial to minimize the recombination effect of the charge carriers, *via* creating trapping species within the transfer route of the charge carriers (Ali et al., 2017; Foura et al., 2017). In order to better illustrate the role of the Fe^{3+} ions in enhancing the light absorption capacity of the BEA/TiO_2, hence enhancing its photocatalytic activity, we propose a localized surface plasmon resonance mechanism (LSPR) as previously reported by Maksod et al. (2017). Fe^{3+} ions exchanged with Na^+ cations in the zeolite and impregnated on the surface of the TiO_2 absorb the visible light irradiation and form excited electrons. These electrons, due to LSPR, move into the conduction band (CB) of the TiO_2 creating positive holes in the iron ions. The transferred electrons result in the formation of the superoxide anion radicals $O_2^{\bullet-}$ that are eventually converted into $\bullet HO_2$ radicals. These $\bullet HO_2$ radicals are further transformed into hydroxyl radicals ($\bullet OH$), which are key radicals for the photocatalytic degradation and complete mineralization of the TC (Jalloul et al., 2021).

In regard to the role of the zeolite, we explain that its presence enhanced the performance of the TiO_2 by increasing its surface area, hence increasing the adsorption of the pollutant molecules on the surface of the catalyst. Moreover, we propose that the zeolite had possibly as well inhibited the recombination effect of the charge carriers. For example, it was suggested that the surface of the zeolite can get saturated with electrons, hence can eventually act as a positive hole entrapper, which would consequently enhance the electron transfer into TiO_2 (Rahman et al., 2018). Another significant role of the zeolite support was to prevent the aggregation of the TiO_2 particles. Liu et al. (2018) and Saadati et al. (2016b) reported that the immobilization of TiO_2 on the zeolite enhanced its efficiency as a photocatalyst by minimizing the aggregation of the TiO_2 particles due to their uniform dispersion on the zeolite.

Moreover, **Figure 7** shows that an increase in the catalyst concentration from 100 mg/L to 250 mg/L under 10 W, enhanced the overall photocatalytic performance of both the unmodified and modified TiO_2, from 54% to 70% and from 77% to 90%, respectively. We mainly attribute this to the increase in the active sites of Fe-TiO_2/BEA due to the increase in the catalyst's concentration; which in turn led to an increase in the absorption of the light photons as well as the adsorption of the pollutant molecules. Higher number of hydroxyl and superoxide active radicals were then eventually generated by

the increased number of charge carriers, leading to an increase in the number TC molecules degrading during the same reaction time (Ebrahimi et al., 2020). Kanakaraju et al. (2014) reported enhanced efficiency of zeolite supported TiO_2 in the degradation of amoxicillin with an increase in the catalyst concentration up to 2 g/L, in agreement with the reporting of Ebrahimi et al. (2020) on the degradation of microcystin by zeolite immobilized TiO_2.

3.2.2.2 Effect of Light Intensity

Figure 8 shows the photocatalytic degradation of tetracycline over TiO_2 and Fe-TiO_2/BEA under 10 W and 50 W blue LED light at an initial concentration of 250 mg/L. As compared to 10 W blue light, the performance of both catalysts under 50 W LED light was higher while the effect was more significant for the Fe-TiO_2/BEA. The efficiency of the Fe-TiO_2/BEA under 50 W was 100% after 90 min compared to only 60% under 10 W. For TiO_2, its photocatalytic degradation efficiency under 50 W was only slightly higher, ~40% after 90 min compared to 38% under 10 W light, which was in agreement with the UV-VIS DRS results, where Fe-TiO_2/BEA exhibited a higher light absorption as compared to the unmodified TiO_2.

Specifically for the Fe-TiO_2/BEA, increasing the intensity of the light improved the photocatalytic degradation efficiency of the system. We attribute this to the generation of more electron/hole pairs in the iron metals, higher number of transferred electrons into the CB of TiO_2, and eventually to the increased number of the active radicals. The effect of light intensity was previously discussed by Hussein (2012), who reported that under low (0–20 mW/cm^2) and intermediate (25 mW/cm^2) light intensities, the rate of the photocatalytic degradation increased linearly with a first order and half order, respectively. Similar results were obtained by Chen et al. (2019) and Das and Ahn (2022) who reported improved photocatalytic degradation of trichloroethylene and TC respectively as a result of increasing the power of the LED light.

To compare our observations with other results reported in literature, we collected and listed in **Table 2** various studies including modified TiO_2 for the photocatalytic degradation of pollutants under visible and Blue LED lights. When analyzing the reported results by other studies using zeolite immobilized catalysts for the degradation of antibiotics like ciprofloxacin (Liu et al., 2017), and oxytetracycline (Al-Harbi et al., 2015), we observe that increasing the power of the LED light source from 50 W (Liu et al., 2017) to 200 W (Al-Harbi et al., 2015) while using the same catalyst greatly enhanced the overall efficiency of the catalyst. In our work, we achieved 100% degradation efficiency for TC after 90 min, employing relatively low-power blue LED light of 50 W. These results are considered to be better when compared to those reported by Liu et al. (2017), for example, who reported 98% degradation of the oxytetracycline over TiO_2-Fe_2O_3/Fe-doped zeolite X catalyst employing 200 W of blue LED light or Liu et al. (2017), who achieved 100% degradation of the ciprofloxacin antibiotic using 50 W LED, with a single wavelength of 455 nm after 3.5 h.

4 CONCLUSION

In this work, we prepared Fe^{3+}-ion sensitized BEA zeolite supported TiO_2 catalyst for the photo-catalytic degradation of tetracycline antibiotic under blue LED visible light. XRD, FTIR, and SEM confirmed the deposition of TiO_2 mainly on the external sites of the zeolite and partially in its internal sites without modifying its morphology. The immobilized TiO_2 catalyst exhibited higher surface area and better adsorption capacity as compared to the unmodified TiO_2. The presence of Fe metal ions in the final catalyst enhanced its visible light absorption as confirmed by UV-VIS DRS. The photocatalytic degradation performance of Fe-TiO_2/BEA was higher and faster under blue LED light as compared to pure TiO_2. The improved efficiency of Fe-TiO_2/BEA was mainly due to its enhanced visible light absorption, higher surface area, better TC adsorption, and lower charge carriers recombination effect. The photocatalytic degradation results of the TC, over the as-prepared catalyst, confirmed that the coupling of Fe^{3+} ion exchange with zeolite immobilization of TiO_2 can be a promising method to extend the photocatalytic application of TiO_2 semiconductor into visible light and enhance its overall adsorption and harvesting capacity for the pollutant. (Zhao et al., 2013).

DATA AVAILABILITY STATEMENT

The raw data supporting the conclusion of this article will be made available by the authors, without undue reservation.

AUTHOR CONTRIBUTIONS

Conceptualization, CB, and HA; Experimental work, GJ, AA-M, FC, and AM; Writing—original draft; GJ and AA-M; Review and editing; CB and HA; Supervision, CB and HA; Funding acquisition, CB. All authors have read and agreed to the published version of the manuscript.

FUNDING

Funding was provided by the WEFRAH (Water-Energy-Food-Health Nexus) initiative at the American University of Beirut (project number: 25202, award number: 103763) and by the University Research Fund (URB) at the American University of Beirut.

ACKNOWLEDGMENTS

The authors gratefully acknowledge the financial support provided by the WEFRAH initiative and the University Research Board at the American University of Beirut.

REFERENCES

Aghajari, N., Ghasemi, Z., Younesi, H., and Bahramifar, N. (2019). Synthesis, Characterization and Photocatalytic Application of Ag-Doped Fe-ZSM-5@ TiO2 Nanocomposite for Degradation of Reactive Red 195 (RR 195) in Aqueous Environment under Sunlight Irradiation. *J. Environ. Health Sci. Engineer* 17 (1), 219–232. doi:10.1007/s40201-019-00342-5

Al-Harbi, L. M., Kosa, S. A., Abd El Maksod, I. H., and Hegazy, E. Z. (2015). The Photocatalytic Activity of TiO2-Zeolite Composite for Degradation of Dye Using Synthetic UV and Jeddah Sunlight. *J. Nanomater.* 2015, 565849. doi:10.1155/2015/565849

Ali, T., Tripathi, P., Azam, A., Raza, W., Ahmed, A. S., Ahmed, A., et al. (2017). Photocatalytic Performance of Fe-Doped TiO2nanoparticles under Visible-Light Irradiation. *Mater. Res. Express* 4 (1), 015022. doi:10.1088/2053-1591/aa576d

Almeida, L. A., Dosen, A., Viol, J., and Marinkovic, B. A. (2022). TiO2-Acetylacetone as an Efficient Source of Superoxide Radicals under Reduced Power Visible Light: Photocatalytic Degradation of Chlorophenol and Tetracycline. *Catalysts* 12 (2), 116. doi:10.3390/catal12020116

Alpatova, A., Meshref, M., McPhedran, K. N., and El-Din, M. G. (2015). Composite Polyvinylidene Fluoride (PVDF) Membrane Impregnated with Fe2O3 Nanoparticles and Multiwalled Carbon Nanotubes for Catalytic Degradation of Organic Contaminants. *J. Membr. Sci.* 490, 227–235. doi:10.1016/j.memsci.2015.05.001

AttariKhasraghi, N., Zare, K., Mehrizad, A., Modirshahla, N., and Behnajady, M. A. (2021). Achieving the Enhanced Photocatalytic Degradation of Ceftriaxone Sodium Using CdS-G-C3n4 Nanocomposite under Visible Light Irradiation: RSM Modeling and Optimization. *J. Inorg. Organomet. Polym. Mater.* 31 (7), 3164–3174. doi:10.1007/s10904-021-01967-6

Bazargan, M. H., Byranvand, M. M., and Kharat, A. N. (2012). Preparation and Characterization of Low Temperature Sintering Nanocrystalline TiO2 Prepared via the Sol-Gel Method Using Titanium(IV) Butoxide Applicable to Flexible Dye Sensitized Solar Cells. *Int. J. Mater. Res.* 103 (3), 347–351. doi:10.3139/146.110644

Behravesh, S., Mirghaffari, N., Alemrajabi, A. A., Davar, F., and Soleimani, M. (2020). Photocatalytic Degradation of Acetaminophen and Codeine Medicines Using a Novel Zeolite-Supported TiO2 and ZnO under UV and Sunlight Irradiation. *Environ. Sci. Pollut. Res.* 27 (21), 26929–26942. doi:10.1007/s11356-020-09038-y

Bel Hadjltaief, H., Omri, A., Ben Zina, M., and Da Costa, P. (2015). Titanium Dioxide Supported on Different Porous Materials as Photocatalyst for the Degradation of Methyl Green in Wastewaters. *Adv. Mater. Sci. Eng.* 2015, 759853. doi:10.1155/2015/759853

Casado, C., Timmers, R., Sergejevs, A., Clarke, C. T., Allsopp, D. W. E., Bowen, C. R., et al. (2017). Design and Validation of a LED-Based High Intensity Photocatalytic Reactor for Quantifying Activity Measurements. *Chem. Eng. J.* 327, 1043–1055. doi:10.1016/j.cej.2017.06.167

Chen, C.-J., Wu, C., Hsieh, L., and Chen, K. (2019). Treatment of Trichloroethylene with Photocatalyst-Coated Optical Fiber. *Water* 11 (11), 2391. doi:10.3390/w11112391

Chong, M. N., Tneu, Z. Y., Poh, P. E., Jin, B., and Aryal, R. (2015). Synthesis, Characterisation and Application of TiO2-Zeolite Nanocomposites for the Advanced Treatment of Industrial Dye Wastewater. *J. Taiwan Inst. Chem. Eng.* 50, 288–296. doi:10.1016/j.jtice.2014.12.013

Cunff, J., Tomašić, V., and Gomzi, Z. (2015). Preparation and Photoactivity of the Immobilized TiO2/chitosan Layer. *Chem. Eng. Trans.* 43, 865–870.

Cunha, D. L., Kuznetsov, A., Achete, C. A., Machado, A. E. d. H., and Marques, M. (2018). Immobilized TiO2 on Glass Spheres Applied to Heterogeneous Photocatalysis: Photoactivity, Leaching and Regeneration Process. *PeerJ* 6, e4464. doi:10.7717/peerj.4464

Das, S., and Ahn, Y. H. (2022). Synthesis and Application of CdS Nanorods for LED-Based Photocatalytic Degradation of Tetracycline Antibiotic. *Chemosphere* 291, 132870. doi:10.1016/j.chemosphere.2021.132870

Ebrahimi, A., Jafari, N., Ebrahimpour, K., Nikoonahad, A., Mohammadi, A., Fanaei, F., et al. (2020). The Performance of TiO2/NaY-Zeolite Nanocomposite in Photocatalytic Degradation of Microcystin-LR from Aqueous Solutions: Optimization by Response Surface Methodology (RSM). *Environ. Health Eng. Manag.* 7 (4), 245–256. doi:10.34172/ehem.2020.29

El-Sherbiny, S., Morsy, F., Samir, M., and Fouad, O. A. (2014). Synthesis, Characterization and Application of TiO2 Nanopowders as Special Paper Coating Pigment. *Appl. Nanosci* 4 (3), 305–313. doi:10.1007/s13204-013-0196-y

Foo, K. Y., and Hameed, B. H. (2010). Insights into the Modeling of Adsorption Isotherm Systems. *Chem. Eng. J.* 156 (1), 2–10. doi:10.1016/j.cej.2009.09.013

Foura, G., Chouchou, N., Soualah, A., Kouachi, K., Guidotti, M., and Robert, D. (2017). Fe-Doped TiO2 Supported on HY Zeolite for Solar Photocatalytic Treatment of Dye Pollutants. *Catalysts* 7 (11), 344. doi:10.3390/catal7110344

Hu, G., Yang, J., Duan, X., Farnood, R., Yang, C., Yang, J., et al. (2021). Recent Developments and Challenges in Zeolite-Based Composite Photocatalysts for Environmental Applications. *Chem. Eng. J.* 417, 129209. doi:10.1016/j.cej.2021.129209

Hussein, F. (2012). Photochemical Treatments of Textile Industries Wastewater. *Asian J. Chem.* 24, 5427–5434.

Ibhadon, A., and Fitzpatrick, P. (2013). Heterogeneous Photocatalysis: Recent Advances and Applications. *Catalysts* 3 (1), 189–218. doi:10.3390/catal3010189

Impellizzeri, G., Scuderi, V., Romano, L., Sberna, P. M., Arcadipane, E., Sanz, R., et al. (2014). Fe Ion-Implanted TiO2 Thin Film for Efficient Visible-Light Photocatalysis. *J. Appl. Phys.* 116 (17), 173507. doi:10.1063/1.4901208

Jalloul, G., Keniar, I., Tehrani, A., and Boyadjian, C. (2021). Antibiotics Contaminated Irrigation Water: An Overview on its Impact on Edible Crops and Visible Light Active Titania as Potential Photocatalysts for Irrigation Water Treatment. *Front. Environ. Sci.* 9 (642), 1. doi:10.3389/fenvs.2021.767963

Kanakaraju, D., Kockler, J., Motti, C. A., Glass, B. D., and Oelgemöller, M. (2014). Titanium Dioxide/zeolite Integrated Photocatalytic Adsorbents for the Degradation of Amoxicillin. *Appl. Catal. B: Environ.* 166-167, 45–55. doi:10.1016/j.apcatb.2014.11.001

Khairy, M., and Zakaria, W. (2014). Effect of Metal-Doping of TiO2 Nanoparticles on Their Photocatalytic Activities toward Removal of Organic Dyes. *Egypt. J. Pet.* 23 (4), 419–426. doi:10.1016/j.ejpe.2014.09.010

Lei, P., Wang, F., Gao, X., Ding, Y., Zhang, S., Zhao, J., et al. (2012). Immobilization of TiO2 Nanoparticles in Polymeric Substrates by Chemical Bonding for Multi-Cycle Photodegradation of Organic Pollutants. *J. Hazard. Mater.* 227-228, 185–194. doi:10.1016/j.jhazmat.2012.05.029

Li, F., Jiang, Y., Yu, L., Yang, Z., Hou, T., and Sun, S. (2005). Surface Effect of Natural Zeolite (Clinoptilolite) on the Photocatalytic Activity of TiO2. *Appl. Surf. Sci.* 252, 1410–1416. doi:10.1016/j.apsusc.2005.02.111

Liao, Q., Rong, H., Zhao, M., Luo, H., Chu, Z., and Wang, R. (2021). Interaction between Tetracycline and Microorganisms during Wastewater Treatment: A Review. *Sci. Total Environ.* 757, 143981. doi:10.1016/j.scitotenv.2020.143981

Liu, M., Yu, S., Hou, L., and Hu, X. (2019). Removal of Oxytetracycline by Fe2O3–TiO2/modified Zeolite Composites under Visible Light Irradiation. *J. Mater. Sci. Mater. Elect.* 30. doi:10.1007/s10854-019-01052-2

Liu, M., Zhang, L., Xi, B.-d., Yu, S., Hu, X., and Hou, L.-a. (2017). Degradation of Ciprofloxacin by TiO2/Fe2O3/zeolite Catalyst-Activated Persulfate under Visible LED Light Irradiation. *RSC Adv.* 7 (81), 51512–51520. doi:10.1039/c7ra08475g

Liu, X., Liu, Y., Lu, S., Guo, W., and Xi, B. (2018). Performance and Mechanism into TiO2/Zeolite Composites for Sulfadiazine Adsorption and Photodegradation. *Chem. Eng. J.* 350, 131–147. doi:10.1016/j.cej.2018.05.141

López, P., Guadalupe, J., González Pichardo, O. H., and Alfonso, J. (2021). Photocatalytic Degradation of Metoprolol in Aqueous Medium Using a TiO2/natural Zeolite Composite. *Fuel* 284, 119030. doi:10.1016/j.fuel.2020.119030

Mahdavi, H., Sajedi, M., Shahalizade, T., and Heidari, A. A. (2019). Preparation and Application of Catalytic Polymeric Membranes Based on PVDF/cobalt Nanoparticles Supported on MWCNTs. *Polym. Bull.* 77, 1. doi:10.1007/s00289-019-02983-w

Maksod, I. H. A. E., Al-Shehri, A., Bawaked, S., Mokhtar, M., and Narasimharao, K. (2017). Structural and Photocatalytic Properties of Precious Metals Modified TiO2-BEA Zeolite Composites. *Mol. Catal.* 441, 140–149. doi:10.1016/j.mcat.2017.08.012

Malkhasian, A. Y. S., Izadifard, M., Achari, G., and Langford, C. H. (2014). Photocatalytic Degradation of Agricultural Antibiotics Using a UV-LED

Light Source. *J. Environ. Sci. Health B* 49 (1), 35–40. doi:10.1080/03601234.2013.836871

Mohd Adnan, M. A., Julkapli, N. M., Iman Amir, M. N., and Maamor, A. (2018). Effect on Different TiO2 Photocatalyst Supports on Photodecolorization of Synthetic Dyes: a Review. *Int. J. Environ. Sci. Tech.* 16, 1–4. doi:10.1007/s13762-018-1857-x

Moshoeu, D. E., Sanni, S. O., Oseghe, E. O., Msagati, T. A. M., Mamba, B. B., and Ofomaja, A. E. (2020). Morphological Influence of TiO 2 Nanostructures on Charge Transfer and Tetracycline Degradation under LED Light. *ChemistrySelect* 5, 1037–1040. doi:10.1002/slct.201904311

Mozia, S., Brożek, P., Przepiórski, J., Tryba, B., and Morawski, A. (2012). Immobilized TiO2 for Phenol Degradation in a Pilot-Scale Photocatalytic Reactor. *J. Nanomater.* 2012, 949764. doi:10.1155/2012/949764

Nawawi, W., Zaharudin, R., Ishak, M., Ismail, K., and Zuliahani, A. (2016). The Preparation and Characterization of Immobilized TiO2/PEG by Using DSAT as a Support Binder. *Appl. Sci.* 7, 24. doi:10.3390/app7010024

Oblak, R., Kete, M., Štangar, U. L., and Tasbihi, M. (2018). Alternative Support Materials for Titania Photocatalyst towards Degradation of Organic Pollutants. *J. Water Process Eng.* 23, 142–150. doi:10.1016/j.jwpe.2018.03.015

Praveen, P., Viruthagiri, G., Mugundan, S., and Shanmugam, N. (2014). Sol-gel Synthesis and Characterization of Pure and Manganese Doped TiO2 Nanoparticles - A New NLO Active Material. *Spectrochimica Acta A: Mol. Biomol. Spectrosc.* 120, 548–557. doi:10.1016/j.saa.2013.12.006

Radwan, E. K., Langford, C. H., and Achari, G. (2018). Impact of Support Characteristics and Preparation Method on Photocatalytic Activity of TiO 2/ZSM-5/silica Gel Composite Photocatalyst. *R. Soc. Open Sci.* 5 (9), 180918. doi:10.1098/rsos.180918

Rahman, A., Nurjayadi, M., Wartilah, R., Kusrini, E., Prasetyanto, E. A., and Degermenci, V. (2018). Enhanced Activity of TiO2/Natural Zeolite Composite for Degradation of Methyl Orange under Visible Light Irradiation. *IJTech* 9, 1159. doi:10.14716/ijtech.v9i6.2368

Saadati, F., Keramati, N., and Ghazi, M. M. (2016). Influence of Parameters on the Photocatalytic Degradation of Tetracycline in Wastewater: A Review. *Crit. Rev. Environ. Sci. Tech.* 46 (8), 757–782. doi:10.1080/10643389.2016.1159093

Saadati, F., Keramati, N., and Mehdipour ghazi, M. (2016). Synthesis of Nanocomposite Based on Semnan Natural Zeolite for Photocatalytic Degradation of Tetracycline under Visible Light. *Adv. Environ. Tech.* 2 (2), 63–70.

Saiful Amran, S. N. B., Wongso, V., Abdul Halim, N. S., Husni, M. K., Sambudi, N. S., and Wirzal, M. D. H. (2019). Immobilized Carbon-Doped TiO2 in Polyamide Fibers for the Degradation of Methylene Blue. *J. Asian Ceram. Societies* 7 (3), 321–330. doi:10.1080/21870764.2019.1636929

Saqib, N., Adnan, R., and Shah, I. (2019). Zeolite Supported TiO2 with Enhanced Degradation Efficiency for Organic Dye under Household Compact Fluorescent Light. *Mater. Res. Express* 6. doi:10.1088/2053-1591/ab2eb8

Sarafraz, M., Sadeghi, M., Yazdanbakhsh, A., Amini, M. M., Sadani, M., and Eslami, A. (2020). Enhanced Photocatalytic Degradation of Ciprofloxacin by Black Ti3+/N-TiO2 under Visible LED Light Irradiation: Kinetic, Energy Consumption, Degradation Pathway, and Toxicity Assessment. *Process Saf. Environ. Prot.* 137, 261–272. doi:10.1016/j.psep.2020.02.030

Scaria, J., Karim, A. V., Divyapriya, G., Nidheesh, P. V., and Suresh Kumar, M. (2020). "Carbon-supported Semiconductor Nanoparticles as Effective Photocatalysts for Water and Wastewater Treatment," in *Nano-Materials as Photocatalysts for Degradation of Environmental Pollutants*. Editor P. Singh (Elsevier), 245–278. doi:10.1016/b978-0-12-818598-8.00013-4

Shokrolahi, S., Farhadian, M., and Davari, N. (2019). Degradation of Enrofloxacin Antibiotic in Contaminated Water by ZnO/Fe2O3/Zeolite Nanophotocatalyst. *J. Appl. Res. Water Wastewater* 6 (2), 150–155.

Sponza, D. T., and Koyuncuoglu, P. (2019). Photodegradation of Ciprofloxacin and Ofloxacin Antibiotics and Their Photo-Metabolites with Sunlight. *Clin. Microbiol. Infect. Dis.* 4. doi:10.15761/cmid.1000149

Sun, C., He, P., Pan, G., Miao, Y., Zhang, T., and Zhang, L. (2018). Study on Preparation and Visible-Light Activity of Ag-TiO2 Supported by Artificial Zeolite. *Res. Chem. Intermed* 44 (4), 2607–2620. doi:10.1007/s11164-017-3249-0

Suwannaruang, T., Hildebrand, J. P., Taffa, D. H., Wark, M., Kamonsuangkasem, K., Chirawatkul, P., et al. (2020). Visible Light-Induced Degradation of Antibiotic Ciprofloxacin over Fe-N-TiO2 Mesoporous Photocatalyst with Anatase/rutile/brookite Nanocrystal Mixture. *J. Photochem. Photobiol. A: Chem.* 391, 112371. doi:10.1016/j.jphotochem.2020.112371

Taufiqurrahmi, N., Mohamed, A. R., and Bhatia, S. (2011). Nanocrystalline Zeolite Beta and Zeolite Y as Catalysts in Used palm Oil Cracking for the Production of Biofuel. *J. Nanopart Res.* 13 (8), 3177–3189. doi:10.1007/s11051-010-0216-8

Tayade, R. J., Kulkarni, R. G., and Jasra, R. V. (2007). Enhanced Photocatalytic Activity of TiO2-Coated NaY and HY Zeolites for the Degradation of Methylene Blue in Water. *Ind. Eng. Chem. Res.* 46 (2), 369–376. doi:10.1021/ie060641o

Torres-Palma, R. A., Serna-Galvis, E. A., and Ávila-Torres, Y. P. (2020). "Photochemical and Photocatalytical Degradation of Antibiotics in Water Promoted by Solar Irradiation," in *Nano-Materials as Photocatalysts for Degradation of Environmental Pollutants* (Elsevier), 211–243. doi:10.1016/b978-0-12-818598-8.00012-2

Tsiampalis, A., Frontistis, Z., Binas, V., Kiriakidis, G., and Mantzavinos, D. (2019). Degradation of Sulfamethoxazole Using Iron-Doped Titania and Simulated Solar Radiation. *Catalysts* 9 (7), 612. doi:10.3390/catal9070612

Varma, K. S., Shukla, A. D., Tayade, R. J., Joshi, P. A., Das, A. K., Modi, K. B., et al. (2021). Photocatalytic Degradation of Levofloxacin by Cu Doped TiO2 under Visible LED Light. *Adv. Wastewater Treat.* 102, 182–198. doi:10.21741/9781644901397-7

Wang, W., Xiao, K., Zhu, L., Yin, Y., and Wang, Z. (2017). Graphene Oxide Supported Titanium Dioxide & Ferroferric Oxide Hybrid, a Magnetically Separable Photocatalyst with Enhanced Photocatalytic Activity for Tetracycline Hydrochloride Degradation. *RSC Adv.* 7 (34), 21287–21297. doi:10.1039/c6ra28224e

Wang, Z., Cai, X., Xie, X., Li, S., Zhang, X., and Wang, Z. (2021). Visible-LED-light-driven Photocatalytic Degradation of Ofloxacin and Ciprofloxacin by Magnetic Biochar Modified Flower-like Bi2WO6: The Synergistic Effects, Mechanism Insights and Degradation Pathways. *Sci. Total Environ.* 764, 142879. doi:10.1016/j.scitotenv.2020.142879

Yilmaz, B., Müller, U., Feyen, M., Maurer, S., Zhang, H., Meng, X., et al. (2013). A New Catalyst Platform: Zeolite Beta from Template-free Synthesis. *Catal. Sci. Technol.* 3 (10), 2580–2586. doi:10.1039/c3cy00073g

Zarazua, E., Torres-Martínez, L. M., Sánchez Martínez, D., and Gomez, C. (2017). Photocatalytic Performance of Titanates with Formula MTiO3 (M= Fe, Ni, and Co) Synthesized by Solvo-Combustion Method. *Mater. Res.* 20.

Zhang, F., Wang, X., Liu, H., Liu, C., Wan, Y., Long, Y., et al. (2019). Recent Advances and Applications of Semiconductor Photocatalytic Technology. *Appl. Sci.* 9 (12), 2489. doi:10.3390/app9122489

Zhao, C., Pelaez, M., Duan, X., Deng, H., O'Shea, K., Fatta-Kassinos, D., et al. (2013). Role of pH on Photolytic and Photocatalytic Degradation of Antibiotic Oxytetracycline in Aqueous Solution under Visible/solar Light: Kinetics and Mechanism Studies. *Appl. Catal. B: Environ.* 134-135, 83–92. doi:10.1016/j.apcatb.2013.01.003

Zhong, X., Zhang, K.-X., Wu, D., Ye, X.-Y., Huang, W., and Zhou, B.-X. (2020). Enhanced Photocatalytic Degradation of Levofloxacin by Fe-Doped BiOCl Nanosheets under LED Light Irradiation. *Chem. Eng. J.* 383, 123148. doi:10.1016/j.cej.2019.123148

Conflict of Interest: The authors declare that the research was conducted in the absence of any commercial or financial relationships that could be construed as a potential conflict of interest.